POLITECNICO DI TORINO
Repository ISTITUZIONALE

UAV OBLIQUE PHOTOGRAMMETRY AND LIDAR DATA ACQUISITION FOR 3D DOCUMENTATION OF THE HERCULES FOUNTAIN

(Article begins on next page)

19 April 2024

UAV OBLIQUE PHOTOGRAMMETRY AND LIDAR DATA ACQUISITION FOR 3D DOCUMENTATION OF THE HERCULES FOUNTAIN

Filiberto Chiabrando, Antonia Spanò, Giulia Sammartano, Lorenzo Teppati Losè[*]

Dep. Architecture and Design, Politecnico di Torino, Viale Pier Andrea Mattioli, 39, 10125 Torino (Italy). filiberto.chiabrando@polito.it, giulia.sammartano@polito.it, antonia.spano@polito.it, lorenzo.teppati@polito.it

Abstract

This paper discusses some enhancements concerning 3D modelling, and the integration and comparison of 3D data from aerial and terrestrial sensors, developed by innovative geomatics techniques around the metric documentation of cultural heritage. In archaeology, it is interesting to deal with the considerable advantages of new multi-sensor approaches for the data acquisition and the management phases in terms of the sustainability (automated acquisition, quickness, precision, time and cost cutting). In particular, Unmanned Aerial Vehicles (UAVs) photogrammetry with the joint use of nadir and oblique cameras can be usefully combined with the large-scale details acquired by the terrestrial Light Detection and Ranging (LiDAR) in vast areas or complex objects, especially in mostly vertical sized objects. Here, we will report the results of an integrated 3D survey in an archaeological context in the Piedmont region of Italy. The Hercules Fountain is located in the gardens of the Venaria Reale (a Savoy Royal Palace included in the UNESCO heritage list) and has witnessed several events and historical phases during the past centuries – from its construction in the 16th century to its disuse and decline in the 17th century, right up to the 21st century when it was eventually brought back to light. The goal of the test is the creation of a 3D continuous model of the site for documentation purposes, future consolidation, and enhancement projects finalised for a public promotion. To meet these strategic aims, a terrestrial laser scanning (TLS henceforth) survey has been designed together with multi-flights by a multi-rotor UAV and terrestrial close-range photogrammetry (CRP) acquisition to produce a highly detailed 3D textured model from which we have inferred standard 2D drawings, digital orthoimages, and further 3D products. In conclusion, the entire workflow and the outputs have been compared together to evaluate the effectiveness of each elaboration according to the different goals of the survey.

Key words: 3D documentation, building archaeology, Light Detection and Ranging (LiDAR), Unmanned Aerial Vehicle (UAV), close-range photogrammetry (CRP), oblique cameras

1. Introduction

New strategies coming from 3D multi-sensor metric survey tools prove that the documentation process can reach good levels of sustainability, in the direction of quality of information and detail, both in terms of time and cost. Furthermore, attempts to effectively apply these techniques in archaeological contexts must take into account the importance of their spatial and temporal complexity. This factor, as in the case study presented in this paper, demands the arrangement of a targeted survey project designed to obtain information suitable for different scopes as well as useful data for experts from different branches of knowledge. A good number of researchers in geomatics have recently begun to approach these themes with the aim of improving and adapting themselves to the different needs of sites (Balletti, Guerra, Scocca, & Gottardi, 2015; Lerma, Navarro, Cabrelles, & Villaverde, 2010; Lerma et al., 2011; Remondino, Barazzetti, Nex, Scaioni, & Sarazzi, 2011). The georeferencing of spatial data is an essential incentive for the interoperability of the sets of data recorded in different times, as a continuous part of the whole process of monitoring and preserving cultural Heritage. As is well known, the choice of specific approaches with dedicated sensors leads to related specific outputs in terms of the level of detail requested, and of resources involved. The integration of 3D metric survey techniques is presented here in a complex and unique test site –the Hercules Fountain in Venaria Reale, a UNESCO World Heritage site (see Section 3 for further details). The goals of the project were as follows: the creation of different metric data as 2D representation, aerial orthoimages and 3D surface model, its usefulness as the basis for further analysis, and different projects of restoration, promotion and valorisation. In this case, the stakeholders for the definition of survey planning were the Laboratory of Geomatics for Cultural Heritage of Politecnico di Torino (performer of the survey project) and the Venaria Reale Royal Palace Management Consortium (client of the documentation request). The selected approaches were: the close-range photogrammetry, the LiDAR survey and the UAV photogrammetric acquisition for the creation of the aerial documentation to integrate the terrestrial one.

A complete UAV acquisition with an oblique configuration of the camera was performed with the aim of understanding the real potentiality of the UAV oblique acquisitions for large-scale documentation purposes. The whole system was conceived and based on a topographic network. After the elaboration of data, a comparison between the results from the different techniques was performed in order to measure and to evaluate which products better fit the initial requirements.

---

[*] Corresponding author: Lorenzo Teppati Losè, lorenzo.teppati@polito.it

2. 3D data documentation role in archaeological sites

2.1. Ground-based data acquisition: about LiDAR techniques and terrestrial photogrammetry

In recent years, the improvement of geomatics multi-sensor tools for the acquisition of 3D information has allowed the recording of multiscale data suitable for several applications. For architectural and archaeological documentation purposes, the high-scale dense data are generally acquired using TLS (active sensor) and CRP (passive sensor). The combined use of these two techniques leads to the creation of a complete model rich in metric and non-metric information. In fact, these models allow the study of not only the geometry of the surveyed object but also the assessment of the pathologies (superficial and structural) that affect the object. Other advantages delivered by these integrated methods are the creation of orthoimages and Digital Elevation Models (DEM) and Digital Surface Models (DSM) as well as the standard survey products (2D and 3D representation) (Boehler & Marbs, 2004; Escarcena et al., 2011; Shan & Toth, 2008). In the field of building archaeology, this potential can be better expressed and used for analysis, material and virtual restoration and digital communication (e.g. augmented/virtual reality). Finally, 3D models derived from point clouds can become useful in terms of the state of conservation monitoring (Patias, 2013). Nowadays, 3D Geographic Information System (GIS) and Historic Building Information Modelling (HBIM) are the most promising tools for managing 3D reality–based information stored in a digital updatable and editable database (Baik, Yaagoubi, & Boehm, 2015; Brumana, Bregianni, Georgopoulos, Oreni, & Raimondi, 2013; Landeschi et al., 2016).

2.2. UAVs for aerial photogrammetry: integration of nadir and oblique cameras

In the last few years, UAV platforms have become one of the most employed systems for mapping and 3D modelling issues. The main advantages that these platforms have contributed to the field of archaeological documentation concern the low-cost alternatives to the classical manned aerial photogrammetry technique (Checa, Morales, & Hernández, 2014). Either multi-rotor or fixed-wing UAVs are now able to perform photogrammetric data acquisition with high-resolution digital camera in semi-automatic and autonomous ways. Through the photogrammetric process, point clouds, DSM/DTM (Digital Terrain Models), orthophotos, textured 3D models, and 2D drawing data can be quickly produced with controlled accuracy in order to achieve accurate documentation of the area. Usually, the acquisitions of architectural and archaeological documentation –finalised for the realization of orthophotos– are performed using the camera oriented in the nadir direction (lens axis pointing at nadir). In aerial photogrammetry, much attention is now focussed on the use of oblique images (Rupnik, Nex, & Remondino, 2013, 2014; Wiedemann & More 2012; Xiao, Gerke, & Vosselman, 2012) and the research activities in the geomatics field are even more oriented in the optimisation of algorithms for the use of "non-conventional" views in the photogrammetric process. In particular, the integration of these images allows users to achieve good results in case of objects with a marked development in height, a radial symmetry and more than one main façade; the *Fontana d'Ercole,* presents all these peculiar features.

3. The Hercules Fountain experience

The Reggia di Venaria Reale (Fig. 1) is one of the residences belonging to the Royal House of Savoy and is located 15 km northwest of Turin (Piedmont, Italy). Since 1997, the site has been included in the UNESCO World Heritage List.

Figure 1: A view of the Reggia di Venaria Reale.

The Hercules Fountain is certainly an important piece of the history of the gardens of the royal residence and a significant feature in their evolution. The ruins of the ancient masonries uncovered 11 years ago are now involved in the second step of the restoration project that needs a detailed and complete 3D documentation.

The construction of the Venaria Reale started in the second half of the 17th century; the designer chosen by the Royal Family for this project was Amedeo di Castellamonte (the royal architect of the Savoy family). The Reggia di Venaria was projected to be one of the bases for the royal hunting expeditions and in the first phase, included the palace, the gardens (in the so-called Italian style), the hunting forests and a small village. Starting from 1699, another architect, Michelangelo Garove, presented a new project for the Reggia and its gardens. Between Castellamonte and Garove, a change in the style occurred; the new model for the royal palaces became Versailles and the House of Savoy decided to modify their palace in Venaria. As we will see, the Fontana d'Ercole was also a victim of this transformation. Two other architects –Filippo Juvarra in 1716, and Benedetto Alfieri in 1739– were entrusted with the task of modifying (again) minor or major parts of the complex by the royal family. After 1789, the winds of the French Revolution crossed the Alps and reached the Piedmont; it was the beginning of the final decline of the Reggia di Venaria. Under the rule of Napoleon, Venaria became a barrack, a role that was to be maintained until the end of the Second World War. The process of restoration started only in 1999 and after years of efforts, the Reggia di Venaria was returned to the public in its original magnificence. Today, with 573337 visitors (MiBACT, 2014), it is one of the most visited historical sites in Italy.
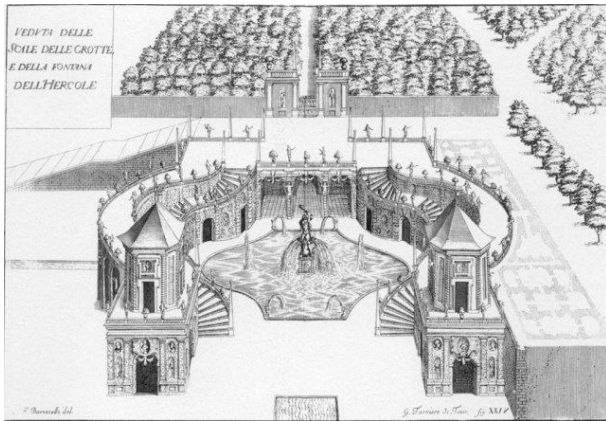
Figure 2: *Fontana d'Ercole.* Drawing of Amedeo di Castellamonte (Castellamonte, 1672).

The *Fontana d'Ercole* was located in the lower gardens and was part of the original project of Amedeo di Castellamonte (Fig. 2). The fountain, built between 1669 and 1672, represented the central architectural and symbolic axis in the main project of the 17th century gardens. Thanks to the two flights of stairs –whose typology is called the "*collo d'oca*"– that run around the large basin, it was intended as the point of connection between the lower garden and the upper garden. The fountain was richly decorated. The walls were covered with mosaics of shells and stones; many sculptures were placed around the basin and the stairs; and the project also included many artificial caves (Fig. 3).

Figure 3: *Fontana d'Ercole*. Drawing of the fountain (Blaeu, 1682). The function of the fountain as connection between the lower gardens and the upper gardens is clearly visible.

Garove was the first to suggest the demolition of the *Fontana d'Ercole* in 1699 (Bruno & Vinardi, 1990) as part of his project for the transformation of the gardens (from an Italian style to a French style). To this end, he wanted to cancel the difference in height between the lower gardens and the upper gardens. The fountain was subjected to a series of demolitions and restorations and was finally dismantled in 1751. The sculptures had the same fate as the fountain; they were collected in the warehouses of Venaria and thereafter scattered among different aristocratic members of the court (a detailed history of the fountain and the sculptures can be found in Cornaglia, 1994). In the summer of 2005, the *Fontana d'Ercole* was uncovered during some excavations in the

gardens (Giacomino, 2005). It was then restored and is now a part of the guided tours of the Reggia.

3.1. Survey operations on the field

At the site of the Hercules Fountain, an integrated 3D survey was conducted in order to acquire different information from multiple sensors. The structure of the masonries is quite complex and irregular; the northern part of the structure, excavated in the last few years, is exposed until the ground level and constrained by the presence of many trees, while the southern area is still underground. Furthermore, the eastern and western parts of the fountain differ in the elevation of the terrain and in the height of the upstanding structures. Finally, all masonries show a significant amount of alteration and have been found to show a generally bad state of conservation, since their architectural coating is almost totally lost. Particular attention was focussed on aerial acquistions, in order to test the influence of the oblique images. These types of acquisition can have a good influence in the process of 3D reconstruction, in particular in complex sites with well preserved structrues (further details and analyses could be found in Aicardi et al., 2016; Chiabrando, Lingua, Maschio, & Teppati Losè, 2017). The collection of data has been carried out in several steps:

- The measurement of the topographic network of the 7 vertices using static GPS/GNSS, and materialised on the terrain by metal nails;

- The measurement of Ground Control Points (GCPs) for the photogrammetric process and scans registration;

- The LiDAR scans (82 acquisitions were performed to cover the whole area);

- The UAV photogrammetric flights (nadir and oblique acquisitions);

- The terrestrial CRP data recording.

3.1.1. Organization of on-site acquisition

As usual, the first step of the fieldwork consisted of the topographic network project. The seven vertices were planned, measured and calculated by static GPS/GNSS receivers (Fig. 4) for georeferencing all the acquisitions from different sensors in the same coordinate system (UTM/WGS84). The topographic network was slightly asymmetric (Fig. 4) compared to the central axis of the fountain. For its positioning, two elements were taken into account: the presence of trees in the northern part of the complex –and the consequent need for two additional vertices for the survey– and the fact that the southern part of the fountain, which is still not excavated, did not need other vertices.

For the acquisition of the laser data, the Focus3D Cam2 by Faro instruments was used (http://www.faro.com/products/3d-surveying/laser-scanner -faro-focus-3d). In the Table 1, the main characteristics of the acquired data are reported.

The distance between the position of the scanner and the walls was always far below the 10 m mark, so an average distance of approximately 3 mm between the points could be assumed. During the operation on the

Table 1: Acquisition data and scan parameters.

No. acquisitions	82
No. registered acquisition	79
Medium no. points/scans	$20 \cdot 10^5$
Resolution (MPti)	1/4 (1 pt/6 mm at 10 m)
Quality	4X
Scan area	360°

(a)
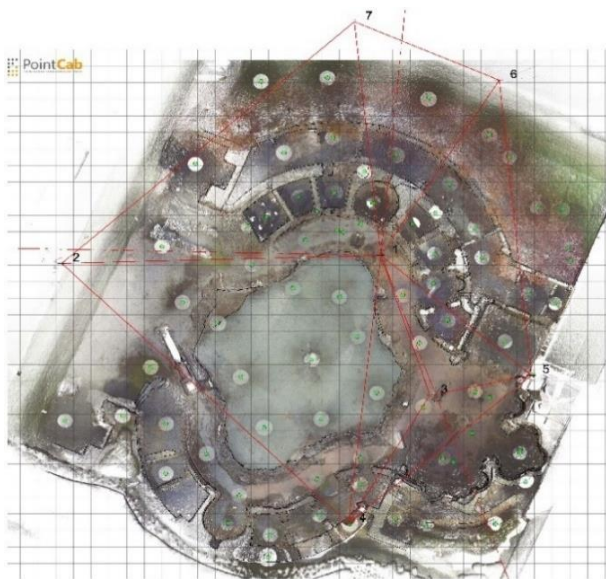
(b)

Figure 4: The GPS/GNSS network: a) acquisition phase; b) planimetric representation of the network vertices.

(a)

(b)

Figure 5: Example of positioning and recording of the targets: a) Topographic measurements using the total station; b) One of the targets placed on the masonries.

(a)

(b)

Figure 6: Examples of bad-quality images: (a) Acquired with lens flare; (b) Affected by large and strong shadows.

field, 82 scans were completed, with a number of points of approximately 20 million for each scan. The Focus3D has an integrated camera that allows the acquisition of the images needed to assign RGB values to every single point of the cloud. For the subsequent phase of the scan registration and also for the photogrammetric processing, many GCPs were placed on the surface of the masonries using paper targets (Fig. 5b). Then, they were measured on the field with a TCR805 by Leica (Fig. 5a) using a traditional total station topographic technique. Afterwards, a close-range photogrammetric acquisition was performed as well. The acquisition was realised in two steps: the first acquired images were recorded during the scan operation in order to have some common markers (GCPs) useful for the orientation of the photogrammetric block. Unfortunately, the quality of these first images –especially in the southern and western part of the fountain– was unclear since the winter sunlight in these parts of the surveyed area was very strong and as a consequence, the acquired images were distorted from the effects of lens flare and large shadows (Fig. 6).

According to these results, a second acquisition campaign was performed on a cloudy day in order to avoid the sun and the problems posed by shadows. In this second step, the radiometric quality of the images

allowed us to consider these data suitable for a complete photogrammetric process. In the second acquisition campaign, no GCPs were placed and recorded. The acquisitions were performed using a Nikon D800E reflex digital camera equipped with a 24 mm lens. The main camera characteristics were as follows: 36 Mpixel CMOS sensor, a max image size of 7360 x 4912 pixels, sensor 36 x 24 mm, and pixel size of 4.89 µm.

The acquisitions were realised according to the shape of the object (Fig. 7) –starting from the basin of the fountain up to the main structures– using very large overlapping (> 80%) between adjacent images, and convergent shoots. To cover the internal part, 457 images were acquired and processed.
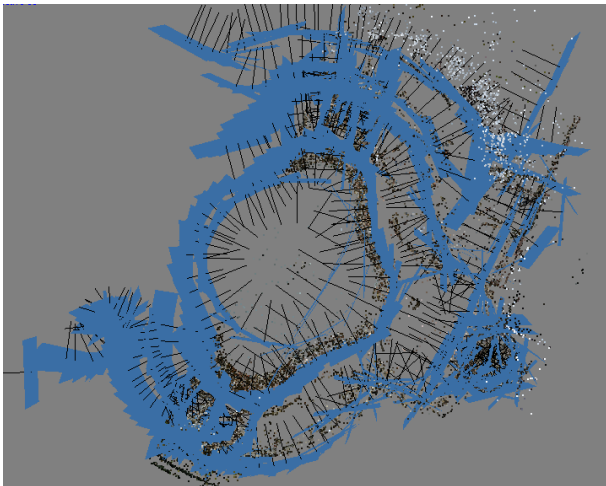

Figure 8: The multi-rotor system.

Figure 7: Terrestrial CRP oriented images.

Figure 9: Ground control station set-up.

The fieldwork was finally completed by three photogrammetric flights performed on the area in order to satisfy the different prerequisites of the survey in terms of scale and the level of detail. The blending of both nadir and oblique acquisitions (Section 3.1.2) allowed the production of a detailed DSM of the fountain with a high-scale detail, especially in the vertical dimension, which was better than that procured through the use of the nadir acquisition only.

The UAV data acquisition was performed using a Hexacopter by Mikrokopter (Fig. 8). The system is composed of six motors and the electronic equipment required for both the remote control and the automatic flight (i.e. one flight control adaptor card; one remote control; one navigation control; one GPS receiver; a three-axis magnetometer; and a wireless connection kit) as well as one computer serving as the ground control station. The Hexacopter has a payload of about 1 kg with a maximum flight time of about 12–15 minutes at a nominal cruise speed 3 to 5 m/s.

As per the configuration employed during the survey, the multi-rotor platform was equipped with a commercial off-the-shelf (COTS) Sony Alpha 5100 digital mirrorless camera with the following main characteristics: 24.3 MPixel CMOS sensor, 6000 x 4000 max. image size, sensor size 23.5 x 15.6 mm, pixel size 3.92 µm, weight 283 g (batteries included) and a 20 mm lens.

The digital camera is mounted on a servo-assisted support that grants electronically controlled rotations along the principal axes. The goal is to acquire vertical imagery (with the lens axis pointing at the nadir position)

for typical photogrammetric acquisitions or oblique images, as well as to point the lens axis according to the predefined direction or to use the integrated first person view (FPV) system that allows the remote visualisation of the acquired area in real time during the flights.

In order to acquire a complete documentation of the fountain for photogrammetric purpose, three flights with a ground sampling distance (GSD) of 0.51 cm were planned and realized in the area. The first planned flight was performed using the typical photogrammetric configuration –camera oriented in the nadir direction and a flight elevation of 30 m above the terrain.

The flight plan was managed by the software Mikrokopter tool OSD that connected the platform to the ground station. The tool was used for setting all the parameters of the flight plan using one of the images made available by several on-line map servers (e.g. Google Maps and Bing Maps) as a reference map of the area. The flight planning approach is the one usually employed and is based on the definition of waypoints (a reference point in the physical space used for the navigation, usually placed at the beginning and at the end of the stripes). According to the general requirements for data processing in the photogrammetric software –which is itself based on structure from motion (SfM) techniques– the overlapping areas among the planned flight lines were approximately > 80 % in longitudinal direction and > 60 % along the lateral part.

According to these characteristics, the flight was performed in about 8 minutes in order to cover all the areas, acquiring the images in 7 flight lines. In the Figures 10 and 11, some screenshots of the planned flight are shown.

As foretold, with the aim of increasing the capacity of documentation and the capacity of exploiting oblique

images that are closely monitored by the geomatics community, two oblique aerial acquisitions were performed as well.

Since the oblique acquisition is still under test and study, a typical strategy does not yet exist. In this paper, we present an acquisition schema provided by the platform in use.

According to the shape of the object, two circular flights with an oblique configuration of the camera were planned and realised. Through the Mikrokopter tools, the available waypoints generator allowed the automatic generation of a fixed number of waypoints (selected by the operator) in a circle in accordance with the centre and the radius chosen in the planning phase (Fig. 11a). This option was used for the oblique positioning performed at a flight elevation of 25 m in order to obtain a GSD comparable to the one obtained by the nadir flight, with a lens axis inclination of 45°.
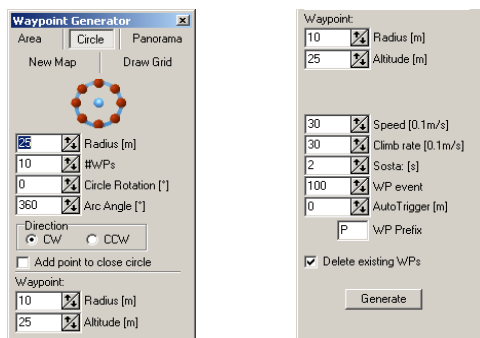
With the presented strategy, the platform would follow the flight plan according to the position of the waypoints: the camera was able to acquire the images with the line of sight oriented to the direction of the central point (p1 in Figs. 11a and 11b). The overlapping between the oblique aerial images was very large (i.e. > 80 %).

(a)

(b)

(c)

Figure 11: Flight planning: a) The nadir flight plan and an example of nadir acquisition; b) Oblique flight plans and an example of oblique acquisition; c) Automatic waypoints generator.

3.1.2. Data processing and 3D modelling

After the network calculation for the definition of the reference system and the EDM (Electronic distance measuring) survey evaluation using traditional topographic software such as Leica Geo Office, Microsurvey, and GeosW, the other acquired data were processed using the following approach.

In the first step, the different scans were registered together (in three different projects for a better management of the data) using the GCPs acquired with the total station; the final achieved accuracy was below 1 cm. This registration was carried out using the Scene Faro software. In the following Table 2, a report of the results of the registration procedure is provided. Thereafter, the whole digital archive derived from TLS was processed into a single point cloud to extract the 2D metric architectural drawings and calculate the 3D model. The 3D Reshaper by Hexagon was the software used to produce a 3D textured surface reproducing the entire fountain, while, for the extraction of planar views (Fig. 12) from the point cloud, Point Cab LSE was used.

Table 2: Scan registration: results and estimated errors.

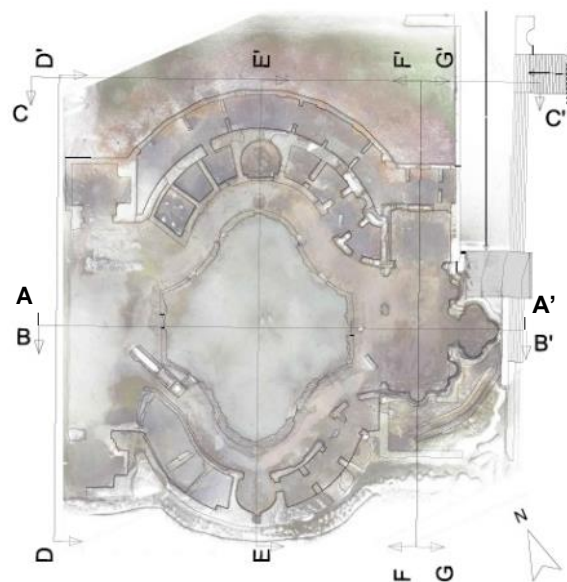|	Mean Target tension (mm)	Mean scan points tension (mm)	Scan points tension < 4 mm
1st group (30scans)	0.008	3.6044	56%
2nd group (22scans)	0.009	5.7302	41.8%
3rd group (27scans)	0.012	4.4945	50.1%
	0.0097	4.6097	49.30%

Figure 12: General plan and indication of elaborated sections.

Thanks to the very high-scale accuracy of the LiDAR model, the level of detail requested for the architectural representation (± 2 cm) could be achieved. Thereafter, an accurate interpretation and drawing were realised using CAD software (Fig. 13).
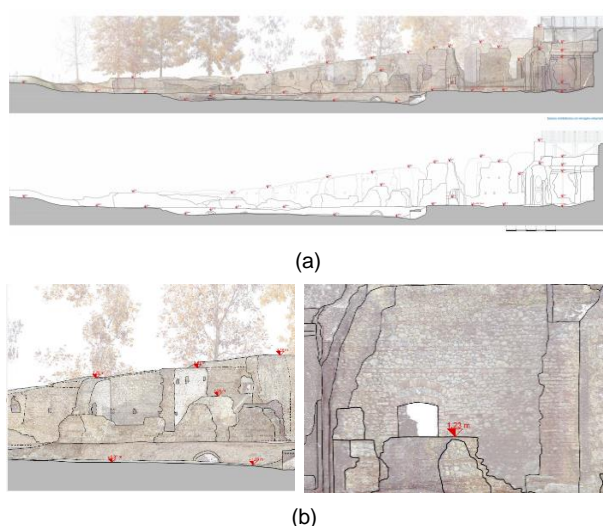
(a)

(b)

Figure 13: Architectonical drawings: a) Sample section (A–A') with and without overlapping orthoimage; b) Examples of detailed views on the drawings.

Furthermore, the terrestrial images collected on the field were processed by a photogrammetric method based on the structure from motion (SfM) approach using Agisoft PhotoScan Professional (v. 1.2.3.2331). Results are showed in Fig. 14. Recalling that the first set of images was not optimal, and that the second set was acquired without GCPs, all the images (and the GCPs) were used to obtain the external orientation parameters.

Subsequently, with the block oriented in the chosen reference system, the photogrammetric products were generated by disabling the first set of images in order to obtain more homogeneous radiometric results.

The results from the photogrammetric process were as follows:

- Area covered – 154 m²

- Average GSD – 1.23 mm/px (pixel size on ground).

- Root mean square (RMS) error on 14 GCPs – 14 mm.

- Final point cloud – almost 100 million points, containng around 9608.06 pt/m².

- Final digital surface – 1.6 million triangles

After the calculation of the terrestrial model, the workflow included the processing of the aerial acquisitions, which was performed with the Pix4D software. We decided to use Pix4D to process the aerial images because, basing on previous experiences (Gini et al., 2013; Whitehead & Hugenholtz, 2015), it is more efficient for the processing of this type of acquisitions. The steps for the generation of the final DSM and orthoimage were the following: camera orientation and tie point (TPs) recognition with the initial processing, images georeferencing using GCPs, point cloud densification, and mesh calculation and texturisation (Strecha, 2014).

Below are the results from the aerial photogrammetric process:

- Area covered – 10700 m²

- Average GSD – 0.51 cm (pixel size on ground)

- RMS error on 29 GCPs – 0.4 cm

- RMS error on 12 ChPs – 0.5 cm

- Final point cloud – almost 71 million points

- Final mesh – almost 10 million triangles

According to the tradition of architectural drawings, an arbitrary level point was assumed at ±0.00 m in the apsidal area of the fountain on the brick floor (corresponding to 252.15 m above sea level).
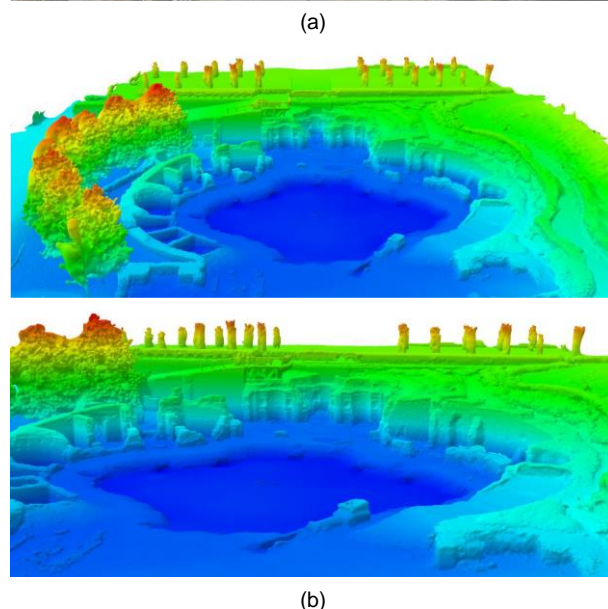

(a)

(b)

Figure 14: The final model: a) A view of the DSM in RGB colours; b) The 3D model textured by an elevation colour ramp.

3.2. Results and data comparison

Since the aims of the 3D survey were the definition of the whole volume and the generation of photogrammetric products useful to the study and analysis of the walls, a comparison between the different results and the techniques employed is now needed. First, for the production of the plan, it was necessary to integrate the terrestrial LiDAR data (Fig. 15) and the orthoimages from the aerial ones. The laser point cloud defined, in a detailed way, all the masonry features using a high-detail scale, thanks also to the scans' positions that were projected in order to cover different levels of the entire fountain area – both in the caves and in the basin. The coverage of the TLS method was generally very good and wide but lacked details in the higher portions of the masonries. Otherwise, the orthoimages from the UAV (Fig. 16), that is generated using the DSM, despite the intrinsically different scale, allowed the filling

(a)

(a)

(b)
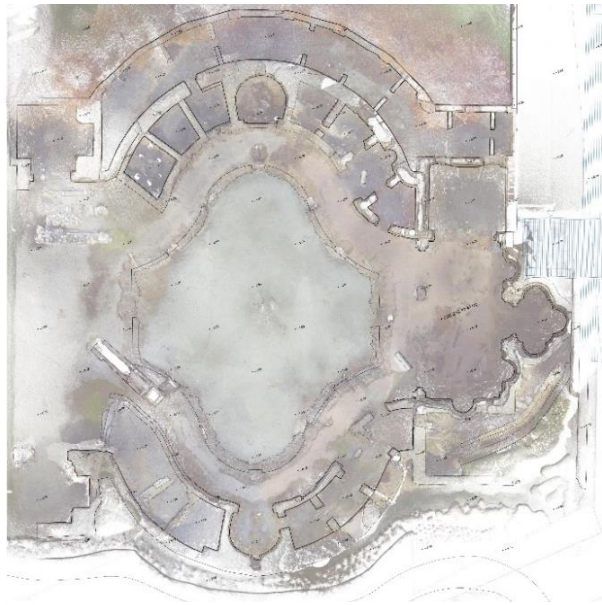
(b)

Figure 15: LiDAR data: a) The orthoimage from laser point cloud; b) A detailed view of drawings derived from the vectorising of TLS point cloud.

Figure 16: Results of UAV photogrammetric process: a) The complete orthoimage of the fountain; b) A zoomed excerpt of the orthoimage.

up of the terrestrial point cloud deficiencies and the generation of a complete 3D model of the site. In fact, for the realisation of the architectural plan, the drawing integrated the information from both the horizontal sections extracted from the point cloud, and the view of the aerial model, i.e. the orthoimage. From the DSM (Fig. 14), after a manual editing and filtering of trees, isolines at the 0.5 m step were extracted as well.

One more interesting consideration pertains to the comparisons between the vertical orthoimages of the apsidal area of the fountain (Fig. 17, section G–G'). This part of the structure was first digitised based on the orthoimage extracted from the TLS point cloud. The achieved detail, as is well known, is typical of the architectural scale and, above all, is set up beforehand according to the chosen scale. Once the drawing phase ended, one of the goals of the research was the quality comparison between LiDAR and CRP orthoimages. Moreover, a comparison among LiDAR, UAVs, and CRP

clouds, using the same portions as sample, was also carried out (Fig. 18).

In detail, four samples from each sensor were chosen to be evaluated (Figures 19-20) in different areas of the fountain, taking into consideration both the vertical extension of the wall and some part of the top of the walls.

First, the point numbers were respectively related to each other, taking into account the density of the acquired data on the fountain surface (Tables 3-6). An example of density mapping by scale colours and the related graph of the distribution of density for the whole sample is reported in this case only for the sample (a) in Figure 21; graphs in Figure 22 show the distribution of the density values. We can assert, considering the Gaussian distribution for the density trend, that the point clouds are very irregular.
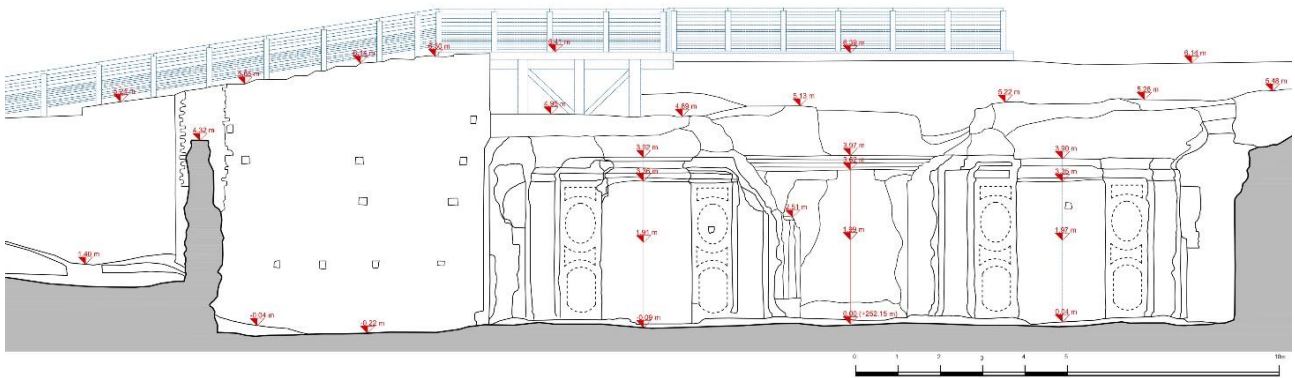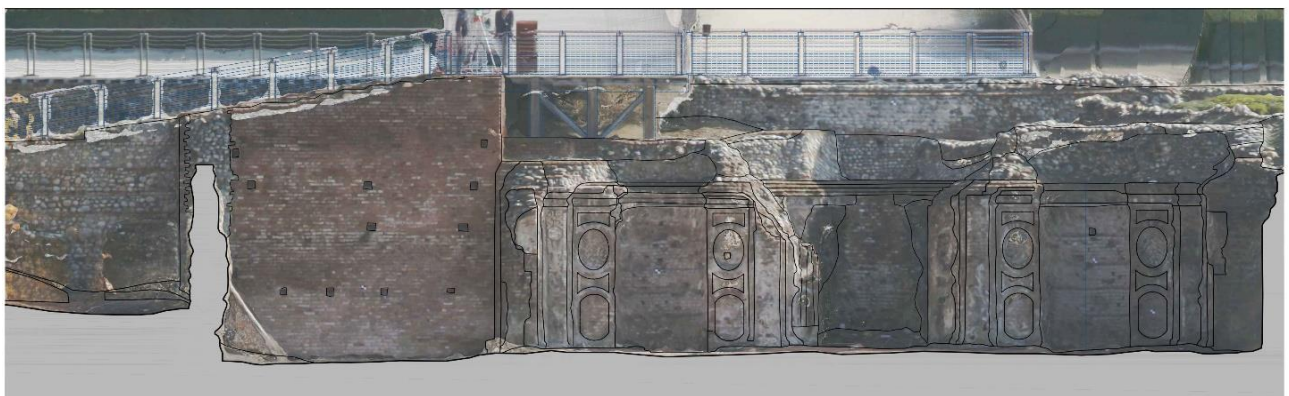
Figure 17: The digitalization of the section G–G'

(a)

(b)

(c)

Figure 18: Compared views among different orthoimages: (a) Orthoimage from the TLS method with the relative vectorialization; (b) LiDAR plotting overlapped with the CRP orthoimage; (c) LiDAR plotting overlapped with the UAV orthoimage.
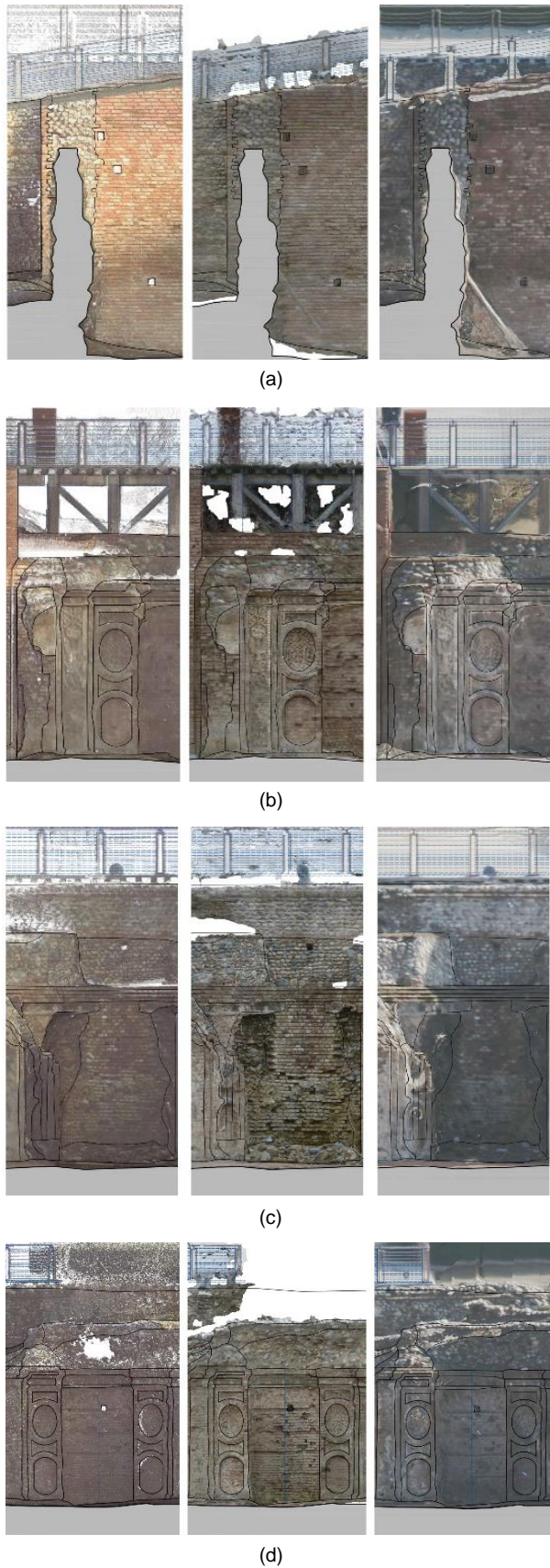
(a)

(b)

(c)

(d)

Figure 19: Four zoomed-in samples chosen for comparison: a) Masonry wall; b) Pilaster with niches, mixed stones-bricks walls; c) Central apse, mixed stones-bricks walls; d) Lateral apse with the top of the masonry walls. For each test area (in row a, b, c, d), the achieved orthoimages are reported in figures. Laser point cloud orthophoto (left); CRP orthophoto (centre); UAV orthophoto (right).

(a)

(b)   (c)

(d)

Figure 20: Four different point cloud samples.

Table 3: Sample (a) – the masonry wall.

Point cloud features from sensors	No. points	Density (pt/m²)	
		Mean	St. dev.
LiDAR scans	2,617,678	186,995,141	48,538
Close-range photogr.	2,734,377	205,860,453	41,446
UAV photogr.	44,823	3,489,436	1,707

Table 4: Sample (b) – a pilaster with niches, made up of mixed stones and bricks walls.

Point cloud features from sensors	No. points	Density (pt/m²)	
		Mean	St. dev.
LiDAR scans	4,298,071	298,212,594	83,014
Close-range photogr.	1,099,149	109,909,586	48,826
UAV photogr.	47,150	4,172,721	2,062

Table 5: Sample (c) – the central apse, made up of mixed stones and bricks walls.

Point cloud features from sensors	No. points	Density (pt/m²)	
		Mean	St. dev.
LiDAR scans	16,183,179	546,717,375	201,170
Close-range photogr.	7,320,709	254,954,953	55,506
UAV photogr.	84,508	3,138,355	1,511

Table 6: Sample (d) – the lateral apse, made up of mixed stones and bricks walls, on the horizontal area at the top of the walls.

Point cloud features from sensors	No. points	Density (pt/m²)	
		Mean	St. dev.
LiDAR scans	10,090,281	357,962,718	355,414
UAV photogr.	242,968	6,162,504	2,065

Table 7: Results from the comparison between point clouds. CRP and UAV photogrammetry were matched to LiDAR through the "*Compute cloud / cloud distance*" tool in the Cloud Compare software. Colour scale mapping and graphs are provided below.

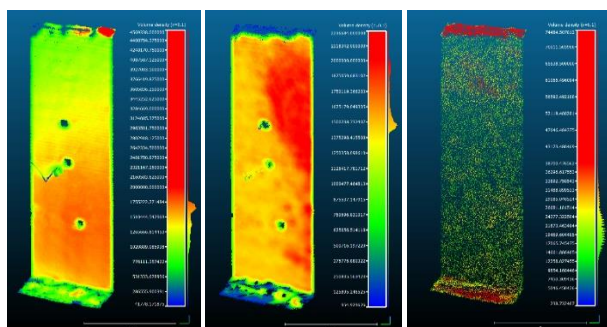|	Absolute distances (m)							
	Sample (a)		Sample (b)		Sample (c)		Sample (d)	
	Mean	St. dev.	Mean	St. dev.	Mean	St. dev.	Mean	St. dev.
LiDAR-CRP	0.012	0.007	0.009	0.011	0.004	0.003	-	-
LiDAR-UAV	0.016	0.013	0.017	0.021	0.021	0.030	0.014	0.015

Figure 21: Example of density analysis on Sample (a): point clouds from LiDAR (left); CRP (centre); UAV point cloud (right). Laser and CRP points are much denser than UAV ones. For example, for the masonry wall in Sample (a): up to 180000 pt/m² laser; CRP 200000 pt/m²; UAV photogrammetry 3500 pt/m².
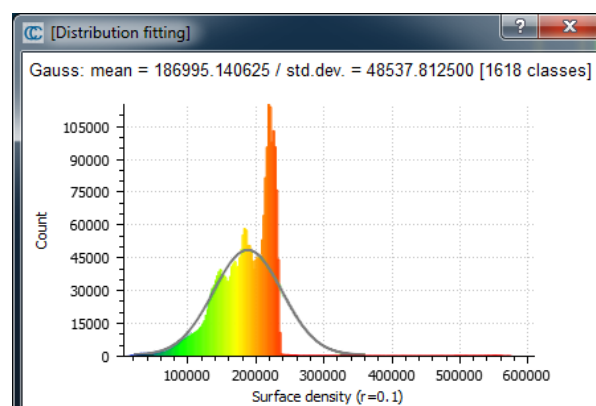
(a)
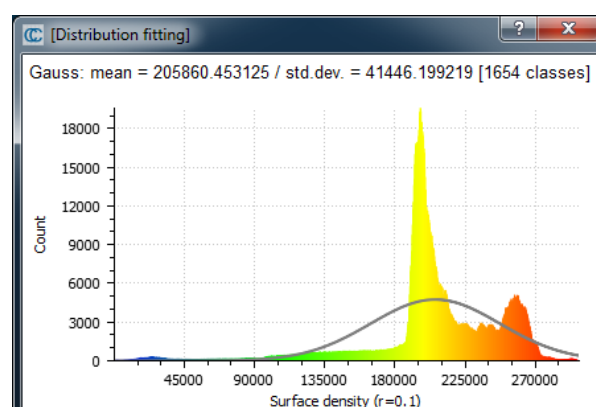
(b)
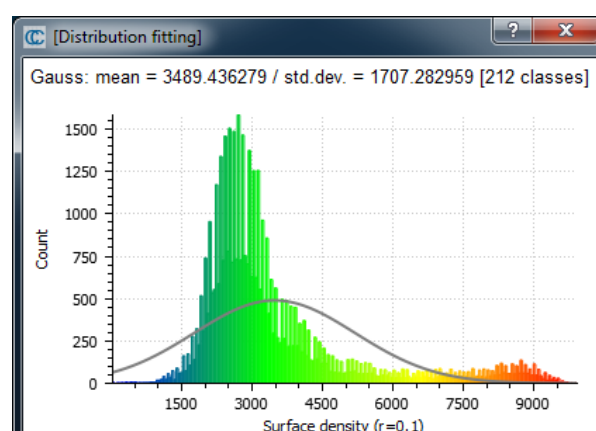
(c)

Figure 22: Statistic distribution of surface density values on Sample (a): a) point clouds from LiDAR; b) CRP; c) UAV. They show the rather non-uniform trend of density in the point cloud as the Gaussian curve, very flat (mean density of 200000 pt/m² and std.dev. of 40000 for CRP) compared to the LiDAR one (mean density of 180000 pt/m² and std.dev. of 50000).

The results in Table 7 display low discrepancies between clouds –as is more expected from CRP than from UAV– according to the different levels of detail reached by the two sensors.

The fourth example (Figure 19) concerns the ridge portion of the wall –more distributed on the horizontal plane and not easily covered by laser scanning survey– in which the contribution of the UAV acquisition was very important and crucial. In Figure 26, the graphic and numerical comparisons are reported.
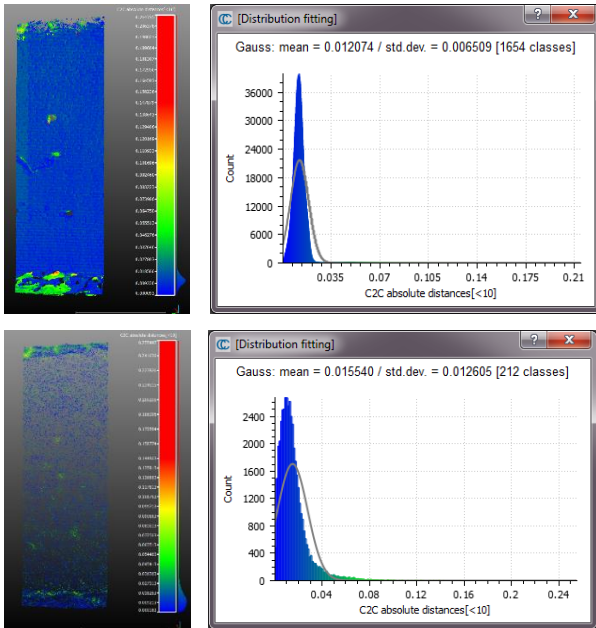
Figure 23: Comparison of point cloud on Sample (a): CRP–LiDAR (up); UAV photogrammetry–LiDAR (down). Difference between the two clouds: 12 mm for CRP and 16 mm for UAV (see Table 6).
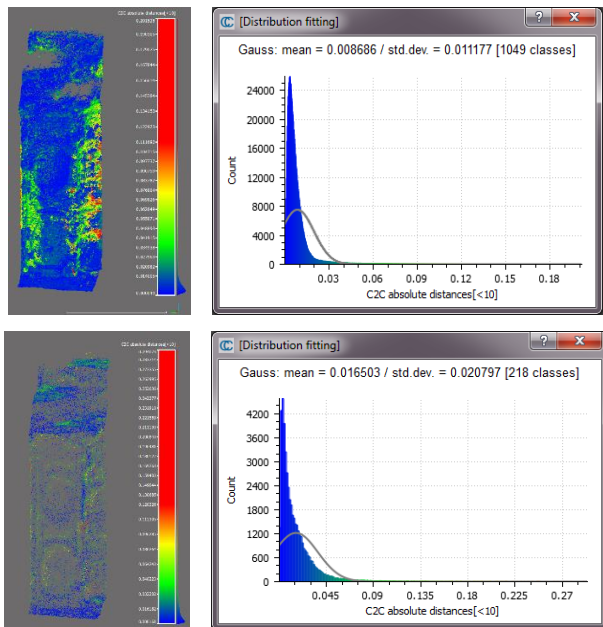

Figure 24: Comparison of point cloud on Sample (b): CRP–LiDAR (up), UAV photogrammetry–LiDAR (down). Difference between the two clouds: 9 mm for CRP and 17 mm for UAV (see Table 6).

4. Conclusions

In case of complex objects or sites, the integration of multi-sensor data can be adopted as the best solution for a multiscale 3D documentation. In fact, the level of detail offered by the three approaches applied in the case study, if distinctly evaluated, is indeed different, and their scales are diverse too. Each result presented above has its own pros and cons (as reported in Section 3.2) in terms of image quality, richness of information, and the time and resources consumed (human, software, and hardware) to achieve the desired results.
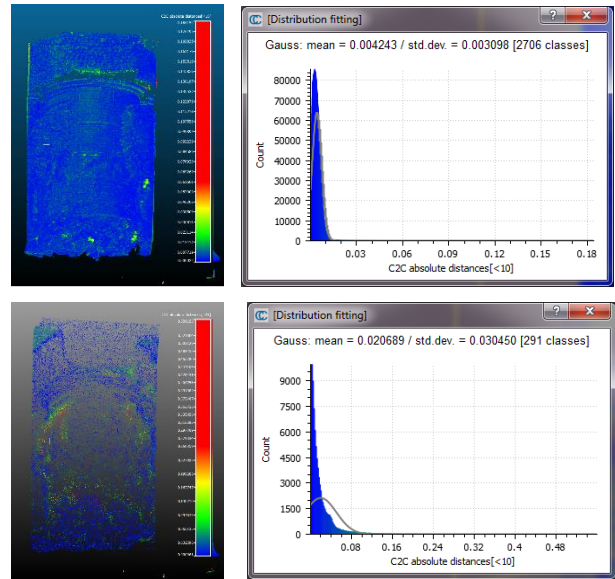

Figure 25: Comparison of point cloud on Sample (c): CRP-LiDAR (up); UAV photogrammetry-LiDAR (down). Difference between the two clouds: 4 mm for CRP and 21 mm for UAV (see Table 6).
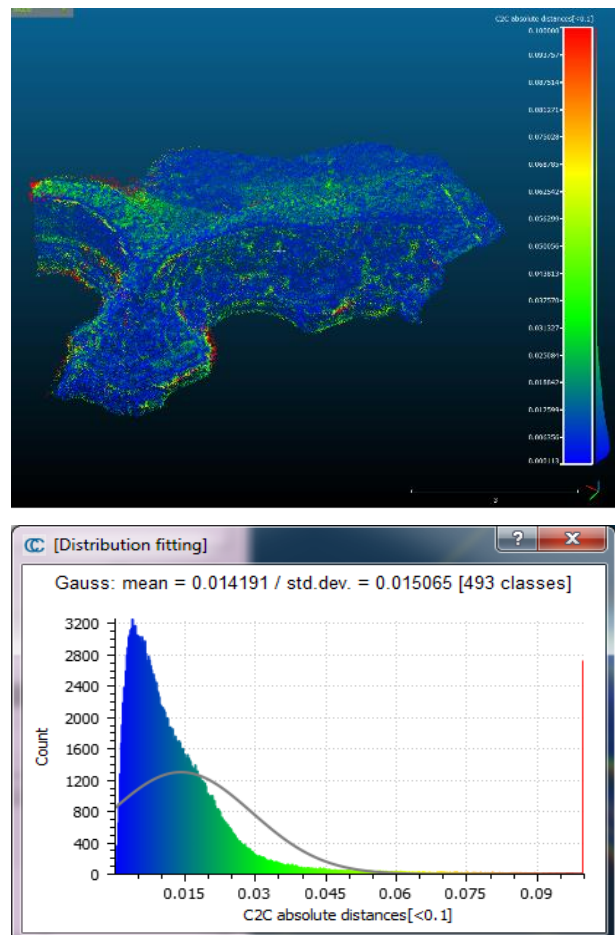

Figure 26: Comparison of point cloud on Sample (d): UAV photogrammetry–LiDAR (up). Difference between the two clouds on the graph: 14 mm for UAV.

First, it was observed that the LiDAR technique is less influenced than photogrammetric ones by atmospherical conditions and light. Thus, the selection of this technique depends mostly on the characteristics of the sites and

the time available for the fieldwork. Nevertheless, the use of TLS has to be combined with the camera acquisition for high-quality texturisation of the model. Moreover, the time processing and human involvement in close-range acquisitions can be defined as very competitive factors thanks to the increasingly automated algorithms of digital photogrammetry that are now available, compared to those of laser point cloud managing.

It is important to underline that all these technological improvements in digital photogrammetry software are largely affected by computer hardware configuration, and on the other hand, they are limited whether the computer used is at a medium performance level with a standard hardware configuration.

The geometrical definition provided from the UAV photogrammetry process is radically different in terms of scale, but this technique reaches a good definition of DSM thanks to the combination of nadir and oblique cameras, now increasingly used in research applications. In the case of the *Fontana D'Ercole* the use of oblique images was of great help in the improvement of the quantity and quality of information generated in the point cloud. The combination of the informations obtained through the combined use of nadir and oblique images and the data obtained from CRP and TLS allowed a complete reconstruction of the fountain, in the parts that were not reached by the two terrestrial sensors.

Despite the positive aspects in the integration of data from the different sensors cited above, the textures need to be further enhanced. The presence of lens flare and large shadows largly affected the images and further radiometric correction need to be performed in order to improve the quality of the texture.

Acknowledgements

References

Aicardi, I., Chiabrando, F., Grasso, N., Lingua, A. M., Noardo, F., & Spanò, A. T. (2016). UAV photogrammetry with oblique images: First analysis on data acquisition and processing. *The International Archives of Photogrammetry, Remote Sensing and Spatial Information Sciences*, *41-B1*, 835–842. http://doi.org/10.5194/isprsarchives-XLI-B1-835-2016

Baik A., Yaagoubi R., & Boehm, J. (2015). Integration of Jeddah historical BIM and 3D GIS for documentation and restoration of historical monument. *The International Archives of Photogrammetry, Remote Sensing and Spatial Information Sciences*, *40-5/W7*, 29–34. http://doi.org/10.5194/isprsarchives-XL-5-W7-29-2015

Balletti, C., Guerra, F., Scocca, V., & Gottardi, C. (2015). 3D integrated methodologies for the documentation and the virtual reconstruction of an archaeological site. *The International Archives of Photogrammetry, Remote Sensing and Spatial Information Sciences*, *40-5/W4*, 215-212. http://doi.org/10.5194/isprsarchives-XL-5-W4-215-2015

Blaeu, J. (1682). *Theatrum statuum regiae celsitudinis Sabaudiae ducis, Pedemontii principis, Cypri regis. Pars prima, exhibens Pedemontium, et in eo Augusta Taurinorum, & loca viciniora.* Amsterdam: Joan Blaeu.

Boehler, W., & Marbs A. (2004). 3D scanning and photogrammetry for heritage recording: a comparison. In *Proceedings of the 12th International Conference on Geoinformatics* (pp. 291-298). Sweden: Gavle University Press.

Brumana, R., Bregianni, A., Georgopoulos, A., Oreni, D., & Raimondi, A. (2013). From survey to HBIM for documentation, dissemination and management of built heritage: The case study of St. Maria in Scaria d'Intelvi. *Digital Heritage International Congress, 2013*, Volume 1, 497–504. http://doi.org/10.1260/2047-4970.2.3.433

Bruno, A., & Vinardi, M. G. (1990). La Fontana d'Ercole a Venaria Reale. *Studi Piemontesi,* 19, fasc. II, 395-396.

Castellamonte, A. (1674). *Venaria Reale, Palazzo di Piacere, e di Caccia, ideato dall'Altezza Reale di Carlo Emanuele II Duca di Savoia, Re di Cipro etc. disegnato e descritto dal conte Amedeo di Castellamonte l'anno 1672.* Torino. Bartolomeo Zapatta.

Checa, Z. P., Morales, A. F., & Hernández, L. A. (2014). Combination of low cost terrestrial and aerial photogrammetry: three-dimensional survey of the church of San Miguel in Ágreda (Soria). *Virtual Archaeology Review*, *5*(10), 51–58. http://dx.doi.org/10.4995/var.2014.4210

Chiabrando, F., Lingua, A., Maschio, P., & Teppati Losè, L. (2017). The influence of flight planning and camera orientation in UAVs photogrammetry. A test in the area of Rocca San Silvestro (LI), Tuscany. *The International Archives of Photogrammetry, Remote Sensing and Spatial Information Sciences*, *42-2/W3*, 163–170. http://doi.org/10.5194/isprs-archives-XLII-2-W3-163-2017

Cornaglia, P. (1994). *Giardini di marmo ritrovati. La geografia del gusto in un secolo di cantiere a Venaria Reale (1699-1798).* Torino: Lindau.

Escarcena, J. C., de Castro, E. M., García, J. L. P., Calvache, A. M., del Castillo, T. F., García, J. D., & Castillo, J. C. (2011). Integration of photogrammetric and terrestrial laser scanning techniques for heritage documentation. *Virtual Archaeology Review*, *2*(3), 53–57. http://dx.doi.org/10.4995/var.2011.4605

Giacomino, G. (2005). Venaria, I lavori potrebbero riservare altre sorprese. La Stampa, 25/08/2005. From: http://archivio.lastampa.it/m/articolo?id=cfcf9e875c6ae2bd0a172adfa14e8d05a97131f8 [02/25, 2016]

Gini, R., Pagliari, D., Passoni, D., Pinto, L., Sona, G., & Dosso, P. (2013). UAV photogrammetry: Block triangulation comparisons *The International Archives of the Photogrammetry, Remote Sensing and Spatial Information Sciences*, *40-1/W2*, 157–162. http://doi.org/10.5194/isprsarchives-XL-1-W2-157-2013

Landeschi, G., Dell'unto, N., Lundqvist, K., Ferdani, D., Campanaro, D. M., & Leander Touati, A. M. (2016). 3D-GIS as a platform for visual analysis: Investigating a Pompeian house. *Journal of Archaeological Science*, *65*, 103–113. http://doi.org/10.1016/j.jas.2015.11.002

Lerma, J. L., Navarro, S., Cabrelles, M., & Villaverde, V. (2010). Terrestrial laser scanning and close range photogrammetry for 3D archaeological documentation: the Upper Palaeolithic Cave of Parpalló as a case study. *Journal of Archaeological Science*, *37*(3), 499–507. http:/doi.org/10.1016/j.jas.2009.10.011

Lerma, J. L., Seguí, A. E., Cabrelles, M., Haddad, N., Navarro, S., & Akasheh, T. (2011). Integration of laser scanning and imagery for photorealistic 3D architectural documentation. C.-C. Wang (Ed.) *Laser Scanning, Theory and Applications*, INTECH Open Access Publisher, 413–430. http://doi.org/10.5772/14534

MiBACT, (2014). Rilevazione 2014 Musei, monumenti e Aree Archeologiche statali. Available: http://www.statistica.beniculturali.it/rilevazioni/musei/Anno%202014/MUSEI_TAVOLA8_2014.pdf [02/25, 2016]

Patias, P. (2013). Overview of applications of close-range photogrammetry and vision techniques in Architecture and Archaeology. McGlone, C. (Ed.), *Manual of Photogrammetry* 6th Edition. American Society of Photogrammetry and Remote Sensing, 1093-1107.

Remondino, F., Barazzetti, L., Nex, F., Scaioni, M., & Sarazzi, D. (2011). UAV photogrammetry for mapping and 3D modeling–current status and future perspectives. *The International Archives of the Photogrammetry, Remote Sensing and Spatial Information Sciences*, *38-1/C22*, 25-31. http://doi.org/10.5194/isprsarchives-XXXVIII-1-C22-25-2011

Rupnik, E., Nex, F., & Remondino, F. (2013). Automatic orientation of large blocks of oblique images. *The International Archives of the Photogrammetry, Remote Sensing and Spatial Information Sciences*, 40-1/W1, 299–304. http://doi.org/10.5194/isprsarchives-XL-1-W1-299-2013

Rupnik, E., Nex, F., & Remondino, F. (2014). Oblique multi-camera systems – orientation and dense matching issues. *The International Archives of the Photogrammetry, Remote Sensing and Spatial Information Sciences*, *40-3/W1*, 107–114. http://doi.org/10.5194/isprsarchives-XL-3-W1-107-2014

Shan, J., & Toth, C. (2008). *Topographic Laser Ranging and Scanning: Principles and Processing.* Boca Raton, FL, USA: CRC press.

Strecha, C. (2014). The rayCloud–a vision beyond the point cloud. FIG Congress 2014, *Engaging the Challenges - Enhancing the Relevance*, Kuala Lumpur, Malaysia 16 – 21 June 2014

Whitehead, K., & Hugenholtz, C. H. (2015). Applying ASPRS accuracy standards to surveys from small unmanned aircraft systems (UAS). *Photogrammetric Engineering & Remote Sensing*, *81*(10), 787–793. http://doi.org/10.14358/PERS.81.10.787

Wiedemann, A., & More, J. (2012). Orientation strategies for aerial oblique images. *The International Archives of the Photogrammetry, Remote Sensing and Spatial Information Sciences*, *39-B1*, 185–189. http://doi.org/10.5194/isprsarchives-XXXIX-B1-185-2012

Xiao, J., Gerke, M., & Vosselman, G. (2012). Building extraction from oblique airborne imagery based on robust façade detection. *ISPRS Journal of Photogrammetry and Remote Sensing*, *68*, 56–68. http://doi.org/10.1016/j.isprsjprs.2011.12.006